Rare Metal Materials and Engineering
Volume 52, Issue 10, October 2023
Available online at www.rmme.ac.cn

Science Press

Cite this article as: Jian Haigen, Xiao Kemou, Pai Junjun, et al. Effect of Deformation Annealing on Microstructure, Texture and Properties of 2A12 Aluminum Alloy[J]. Rare Metal Materials and Engineering, 2023, 52(10): 3363-3373.

ARTICLE

Effect of Deformation Annealing on Microstructure, Texture and Properties of 2A12 Aluminum Alloy

Jian Haigen[1,4], Xiao Kemou[1,3], Pai Junjun[2], Chen Miao[1], Zhang Wei[3]

[1] College of Materials and Advanced Manufacturing, Hunan University of Technology, Zhuzhou 412007, China; [2] Shandong Key Laboratory of Advanced Aluminum Materials and Technology, Binzhou 262207, China; [3] Guangdong Fenghua Zhuoli Technology Co., Ltd, Foshan 528200, China; [4] OKE CNC Precision Tool Co., Ltd, Zhuzhou 412500, China

Abstract: The effects of different deformation annealing processes on the microstructure, texture, and properties of 2A12 aluminum alloy were studied by scanning electron microscope (SEM) equipped with energy dispersive spectrometer (EDS) and electron backscatter diffraction (EBSD). Results demonstrate that after deformation annealing treatment, the 2A12 aluminum alloy grains become longer along the rolling path and smaller in size. The proportion of subgrain boundaries decreases, the proportion of low angle grain boundaries (LAGB) at 2°−15° increases, and the proportion of high angle grain boundaries (HAGB, >15°) first increases and then declines as the deformation annealing treatment cycles increase. The degree of recrystallization rises at this point as the annealing process switches from recovery multi-lateralization to recrystallization. After single-step deformation annealing, the two samples have a similar microstructure and proportion of HAGB and LAGB in total due to the small deformation and less deformation stored energy. Compared to the sample that underwent mild deformation with the same annealing process, the large deformation sample has a lower proportion of subgrain boundaries in total and a higher proportion of LAGBs and HAGBs, and the degree of recrystallization increases. There will be texture evolution pathways of Brass→R-Cu and m-Brass→Goss→R-Goss→Cube, T and $P_{0°}$ →Near rotated Cube and {102}<201> when the deformation is significant. R-Cu and m-Brass→Goss→R-Cube will become the new route during single-step small deformation annealing. The toughness and plasticity of the 2A12 aluminum alloy diminish while the strength and hardness rise with higher deformation.

Key words: 2A12 aluminum alloy; deformation annealing; mechanical properties; corrosion property; texture

2A12 aluminum alloy is a typical heat-treatable strengthened high-strength aluminum alloy[1–3], which has many advantages such as low density, high specific strength, low recycling cost, excellent electrical conductivity, easy workability, and welding properties, and has been extensively used in aerospace, transportation, and military industries[4–6]. Deformation annealing is a processing method that combines plastic deformation with heat treatment to improve overall performance by modifying the microstructure and precipitate distribution of the alloy[7–8]. As a result, the deformation annealing process has been one of the most important means for improving the properties of aluminum alloy materials.

The researchers have carried out the deformation annealing processes of aluminum alloys. Wang et al[9] investigated the microstructure and mechanical properties of 2024 aluminum alloy after repeated cold rolling and annealing, and found that the mechanical properties are improved due to the synergetic effect of microstructure densification, grain refinement and dislocations strengthening. Xu[10] studied the microstructure and mechanical properties of cold-rolled and annealed Al-Cu alloys, and discovered that the hardness of the alloys increases linearly with increasing rolling reduction at low strain magnitude, while parabolically and slowly at medium and high strain magnitude. Furthermore, compared to coarse-grained materials, the strength of the Al-Cu alloy material with ultrafine-grained microstructure obtained by intensive plastic deformation is raised by 2–3 times, and the yield point phenomenon is avoided. Hu[11] investigated the effect of rapid

Received date: February 06, 2023
Foundation item: Natural Science Foundation of Hunan Province (2023JJ50174); Project of Industry-University Cooperation and Collaborative Education of Ministry of Education (220506429021607); College Students Research Learning and Innovative Experiment Project (2023176)
Corresponding author: Zhang Wei, Ph. D., Guangdong Fenghua Zhuoli Technology Co., Ltd, Foshan 528200, P. R. China, Tel: 0086-757-88775571, E-mail: zw@fhzl.co

cold punching on the microstructure and mechanical properties of spray formed Al-Cu-Mg alloy and discovered that the change in the hardness of the alloy is primarily influenced by the combination of phase-resolving softening, work hardening, and reprecipitation strengthening. It is clear from the prior studies that the grain size, precipitate size and distribution, dense structure, and dislocation density are critical parameters influencing the mechanical properties of aluminum alloys after deformation annealing.

In addition to mechanical properties, the intercrystalline precipitation obtained after heat treatment will increase the localized corrosion susceptibility and decrease the intercrystalline corrosion resistance of the aluminum alloy[12]. The elongated grains of the aluminum alloys are one of the leading causes for exfoliation corrosion initiation[13], so it is necessary to study the corrosion properties of aluminum alloys after deformation annealing. However, most researches on the corrosion properties of aluminum alloys after deformation annealing are concentrated on 3XXX series[14–15] and 5XXX series aluminum alloys[16–18], with comparatively little research on 2XXX series aluminum alloys. Owing to the aforementioned background, the effects of three different deformation annealing processes on the microstructure, texture, hardness, and corrosion properties of 2A12 aluminum alloy were researched in this work.

1 Experiment

1.1 Material

2A12-T4 aluminum alloy sheet with a thickness of 15 mm was studied in this work. Its main chemical composition is given in Table 1.

The experimental materials were machined into blocks with 150 mm×50 cm×15 mm in dimension. The 2A12 aluminum alloy can be empirically annealed at temperatures between 270 and 450 °C. According to temperature, the annealing procedure can be divided into three groups: low temperature annealing (270–320 °C), partial annealing (320–380 °C), and high temperature annealing (380–450 °C). The annealing method is typically chosen for high-temperature short-time or low-temperature long-time annealing in the actual research and manufacturing process because increasing the annealing temperature and extending the annealing time have a similar effect on the alloy properties. For the cold rolling of low plasticity alloys, the process of cold rolling once and intermediate annealing once is usually chosen. In this study, samples treated with repeated deformation annealing, single-step deformation annealing, and large deformation annealing were selected for a comparative study on microstructure and properties to investigate the effects of different deformation annealing processes on the microstructure and properties of 2A12 aluminum alloy. Repeated deformation annealing process is that the materials are cold rolled by 15% and annealed at 350 °C for 30 min, and these procedures are repeated three times. The materials obtained from different passes were numbered as 11#, 12#, and 13#. Samples 21# and 22# were subjected to the single-step deformation annealing, and they were cold rolled by 5% before being annealed at 280 °C for 72 h and 400 °C for 10 min, respectively. Sample 31# was cold rolled with 50% large deformation and annealed at 350 °C for 30 min, and the detailed process parameters are shown in Table 2.

Table 1 Chemical composition of 2A12 aluminum alloy (wt%)

Cu	Mg	Fe	Si	Zn	Mn	Ti	Al
3.8–4.9	1.2–1.8	≤0.5	≤0.5	≤0.3	0.3–0.9	≤0.15	Bal.

1.2 Testing methods

After deformation annealing, the plates were divided into small pieces with dimensions of 10 mm×10 mm. The sample preparation must involve mechanical pre-grinding and polishing for microstructure observation, phase analysis, and performance testing. Phase analysis was performed on an NKTIMA IV X-ray diffraction with a working voltage of 40 kV, current of 30 mA, a scan speed of 2°/min, scanning step of 0.02°, and a scanning range of 5°–90°.

Samples for EBSD analysis were electropolished in an 5% $HClO_4$+95% C_2H_5OH solution by LP305DE DC regulated power supply at the polishing voltage of 5 V for 3–5 s. Microstructure and texture characterization were carried out using EBSD (Oxford C-nano), and the raw data were analyzed and processed by HKL-Channel 5 software to obtain the crystallographic information of the samples.

The non-test surfaces of the corrosion samples were covered with pourable denture base resin. According to GB/T 22639-2008 standard, the samples were immersed in exfoliation corrosion solution (EXCO, 234 g/L NaCl +50 g/L

Table 2 Deformation annealing process parameters of 2A12 aluminum alloy

Condition	Sample	Rolling reduction/%	Annealing processes	Replicated times	Thickness reduction/mm
T4	01#	-	-	-	-
Repeated deformation annealing	11#	15	350 °C, 30 min	1	15–12.75
	12#	15	350 °C, 30 min	2	15–10.83
	13#	15	350 °C, 30 min	3	15–9.21
Single-step deformation annealing	21#	5	280 °C, 72 h	1	15–14.25
	22#	5	400 °C, 10 min	1	15–14.25
Large deformation annealing	31#	50	350 °C, 30 min	1	15–7.50

KNO_3+ 6.5 mL/L HNO_3) at 25 °C for 96 h. At regular intervals, samples were taken from the solution to observe and to record their visual grade. The corrosion products on the surface of the samples were removed according to GB/T 16545-2015 standard, the samples were weighed, and metallographic image were taken.

According to the GB/T 40299-2021 standard, using a conventional three-electrode system with a Pt electrode as the auxiliary electrode, a saturated calomel electrode (SCE) as the reference electrode, and a working sample as the test electrode, electrochemical tests were performed on a CHI 760E electrochemical workstation with an electrolyte of 3.5% NaCl solution. The raw data were analyzed and processed using ZSimpWin software.

Hardness tests were carried out on an HV-1000 microhardness instrument according to the GB/T 4340.1-2009 standard, and the hardness values of ten random points were tested; the average value was taken as the hardness value of this sample after the maximum and minimum values were removed.

Tensile tests were conducted on a UTM 4204 universal machine according to GB/T 228.1-2010. The dimension of the tensile sample is shown in Fig. 1. Based on the raw data, the tensile strength, yield strength, and elongation of the samples were calculated.

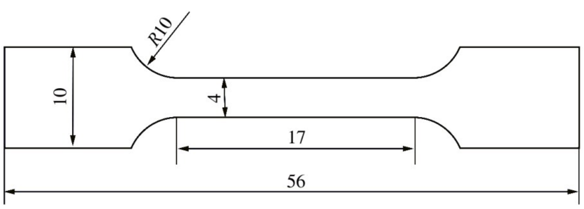

Fig.1 Dimension of tensile sample

2 Results and Discussion

2.1 Phase analysis

Fig. 2 shows an SEM image of sample 11#. During rolling, coarse hard phase particles suffer a brittle fracture and are distributed along the rolling direction[19]. The energy spectrum analysis results in Table 3 show that the short rod-like gray phase is a typical Al_2CuMg phase (S-phase) [12], and the massive silver-white phases are a hard and brittle impurity phase with evident cracks after rolling that may be AlCuFeMn or AlCuFeMnSi multiphase based on its chemical composition.

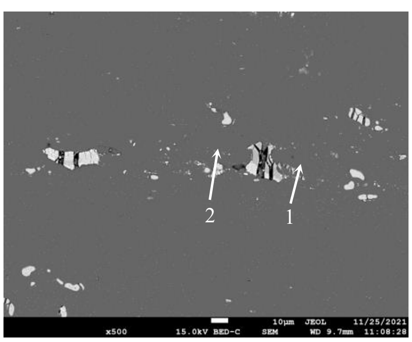

Fig.2 SEM image of sample 11#

Table 3 EDS results of spots marked in Fig.2 (at%)

Spot	Al	Cu	Mg	Mn	Fe	Si	O
1	52.65	24.31	22.06	-	-	-	0.99
2	72.48	16.93	-	5.60	4.77	0.22	-

Fig. 3 shows the XRD patterns of 2A12 alloy samples after different deformation annealing processes. It can be seen that the alloy is mainly composed of α(Al), Al_2CuMg, $Al_{20}Cu_2Mn_3$ (T-phase), and Mg_2Si phases, etc. The Al_2CuMg and Mg_2Si phases are more prevalent in sample 12#, 13#, and 31#, which have undergone large deformation, and the diffraction peak intensity of these phases increases with increasing deformation amount. The Mg_2Si phase diffraction peaks disappear, and the intensity of Al_2CuMg phase diffraction peaks decreases for sample 21# and 22#, which undergo 5% cold rolling deformation. The phenomena mentioned above occur because the large deformation promotes the second phase precipitation in the alloy during annealing, thus increasing the second phase content. In contrast to the second phase in sample 21#, the Al_2CuMg phase diffraction peak in sample 22# is further depressed due to partial dissolution of the low melting point Al_2CuMg phase during high temperature annealing, resulting in a decrease in Al_2CuMg phase content. The fine high melting point $Al_{20}Cu2Mn_3$ phase does not change appreciably during the deformation annealing.

2.2 Effect of repeated deformation annealing on microstructure and texture of 2A12 alloy

2.2.1 Microstructure characteristic

Fig. 4 depicts the IPF map and EBSD analysis results of sample 11#, 12#, and 13#, and different colors represent distinct micro-orientations of grains. Except for a few grains with equiaxed structure, most of the grains are elongated along the rolling direction, showing the typical microstructure of rolling aluminum alloy in an annealing state, as shown in Fig. 4a, 4d, and 4g. In comparison to the samples without deformation annealing as shown in Fig. 5, the grain sizes of

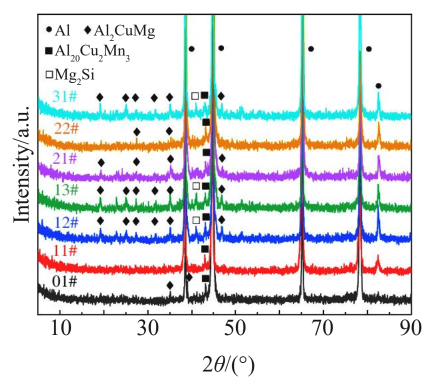

Fig.3 XRD patterns of 2A12 alloy samples

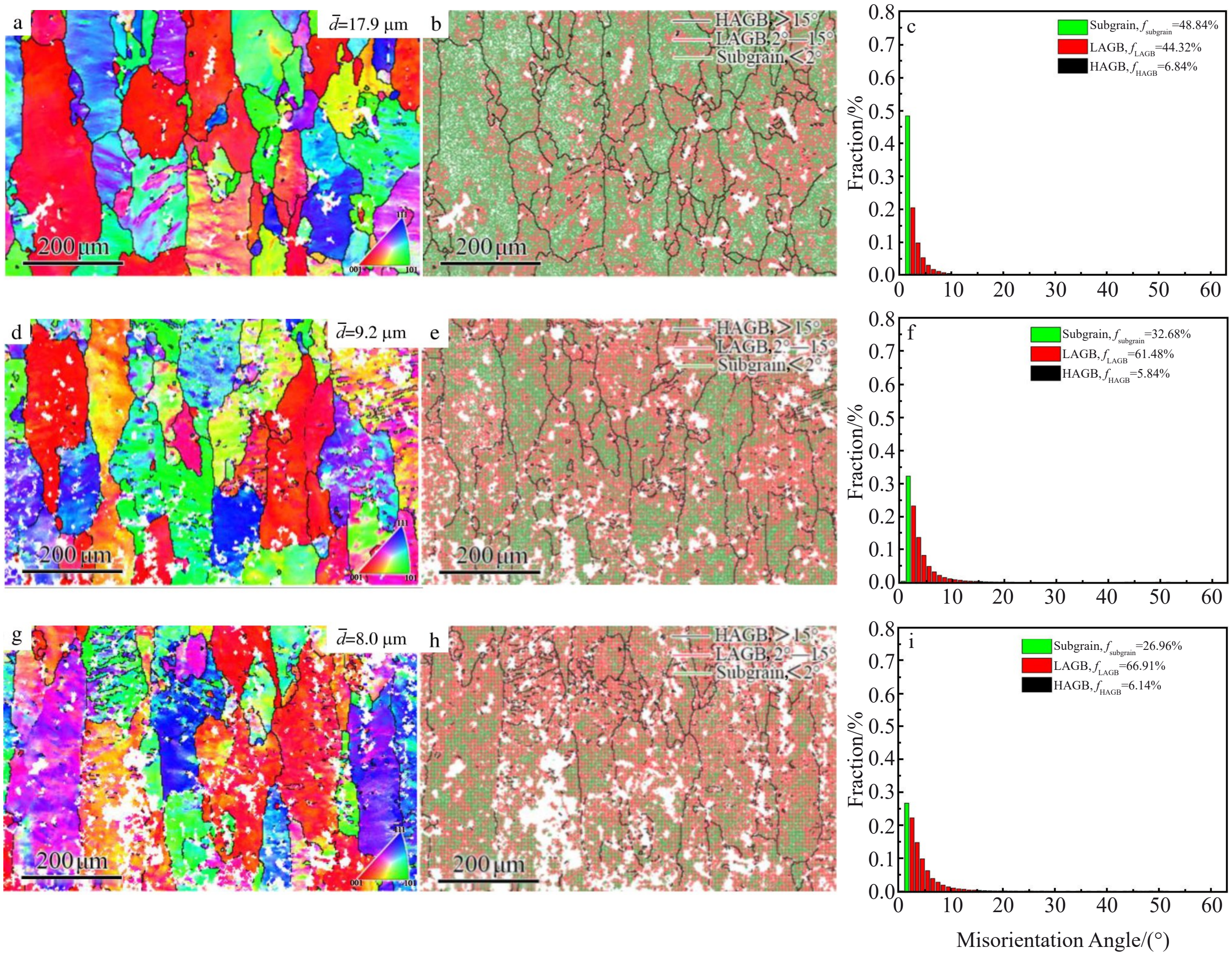

Fig.4 IPF maps, grain boundary maps, and misorientation angle frequency histograms of 2A12 aluminum alloy samples after repeated deformation annealing: (a–c) 11#, (d–f) 12#, and (g–i) 13#

sample 11#, 12#, and 13# are smaller, and the larger the cold rolling, the finer the grains. The above situation happens because some grains are crushed and broken during the deformation process. The broken grain boundaries remain inside the grains and become nucleation points for recrystallization during annealing, increasing the number of recrystallized grains and decreasing the average grain size. The grain shape progressively elongates, the aspect ratio rises, and the degree of fragmentation becomes severer as the cumulative deformation from repeated deformation annealing rises. Additionally, the color inside the large grains starts to look "mottled", which shows that there is a significant local variation in micro-orientation, as shown in Fig.4a, 4d, and 4g.

The grain boundary maps and misorientation angle frequency histograms indicate the distribution and volume proportion of high angle grain boundary (HAGB, >15°) and low angle grain boundary (LAGB, ≤15°). Fig.4b, 4e, and 4h show that the subgrain boundaries and low angle grain boundaries predominate in the three groups of repeated deformation annealed samples, and the proportion of high angle grain boundaries is minimal. The repeated deformation annealing method at 350 °C for 30 min is the primary cause. Low annealing temperatures and brief annealing times result in low recrystallization levels. The misorientation angle frequency histograms of the repeated deformation annealing samples are shown in Fig. 4c, 4f, and 4i. After repeated deformation annealing, the proportion of subcrystal boundaries totally decreases from 48.84% in sample 11# to 26.96% in sample 13#, and the proportion of LAGBs (2–15°) in total increases from 44.32% in sample 11# to 66.91% in sample 13#, and HAGBs change little.

This demonstrates how the degree of grain breakage, local micro-orientation difference, and dislocation density gradually rise as the cumulative deformation from repeated deformation annealing grows. The microstructure primarily experiences partial recrystallization and high temperature recovery during 350 °C annealing of the 2A12 aluminum alloy. The total amount of deformation in the 11# and 12# samples is negligible, and the introduced deformation energy storage is insufficient to induce the recrystallization process. The percentage of HAGBs declines as a result of the multi-lateralization process brought on by high temperature recovery during annealing. The proportion of HAGBs in the 12# and 13# samples rises as the cumulative deformation

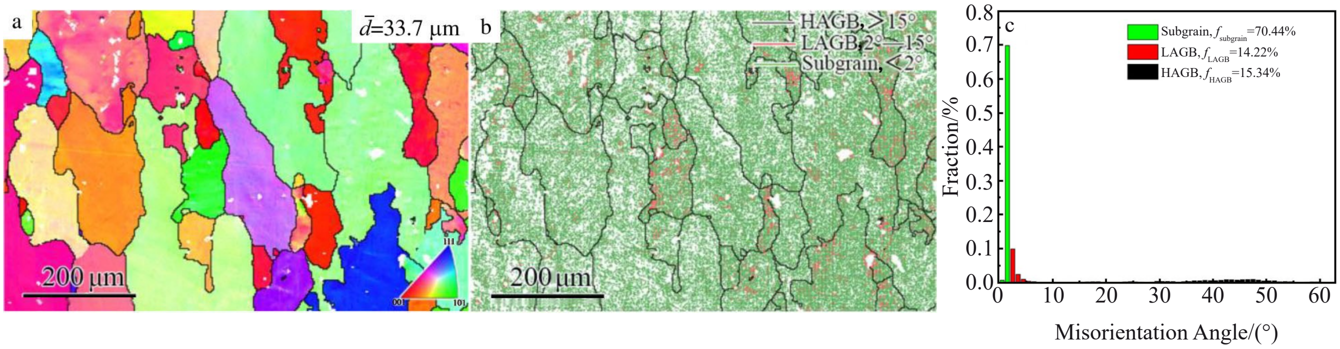

Fig.5 IPF map (a), grain boundary map (b) and misorientation angle frequency histogram (c) of 2A12-T4 aluminum alloy

increases, deformation energy storage is introduced into the sample, and the recrystallization process gradually takes over.

2.2.2 Texture

The orientation distribution function (ODF) of repetitive deformation annealed samples is shown in Fig.6. The Cube, R-Cube, Brass, copper, S, Goss, R, M, and P textures are primary deformation annealing patterns for aluminum alloys. The majority of the current study on aluminum alloy texture focuses on analyzing the aforementioned typical deformation annealing texture. The recovery and early recrystallization of aluminum alloy can result in some atypical intermediate textures and the previous characteristic texture, such as R-Cu and m-Brass textures created by Brass decomposition[20]. The highest texture intensity of the sample 01# is 10.86, as shown in Fig. 6. The majority of the textures are intermediate textures, like m-Brass {211} <0, $\bar{1}$, 1>, $\alpha_{55°}$ {011} <1, $\bar{1}$, 1>, F {111}<112>, {025}<100>, {359}<433>, {4$\bar{5}$2}<012> and $Cu_{35°}$, as shown in Table 4. The highest texture intensity of sample 11# is 7.92 compared to sample 01#. The m-Brass texture intensity drops to 3.35, and the R-Cu texture disappears and is replaced by the Cube, Goss, T, and the near rotated Cube textures. The Cube and Goss textures disappear, the near rotated Cube texture's intensity drops to 6.13, forming the {102} <201> and P textures, and the highest texture intensity of 12# is 6.13. The T and P textures vanish, the near rotatable Cube and {102}<201> texture's intensity is increased to 6.16, and the highest texture intensity of 13# is 8.36.

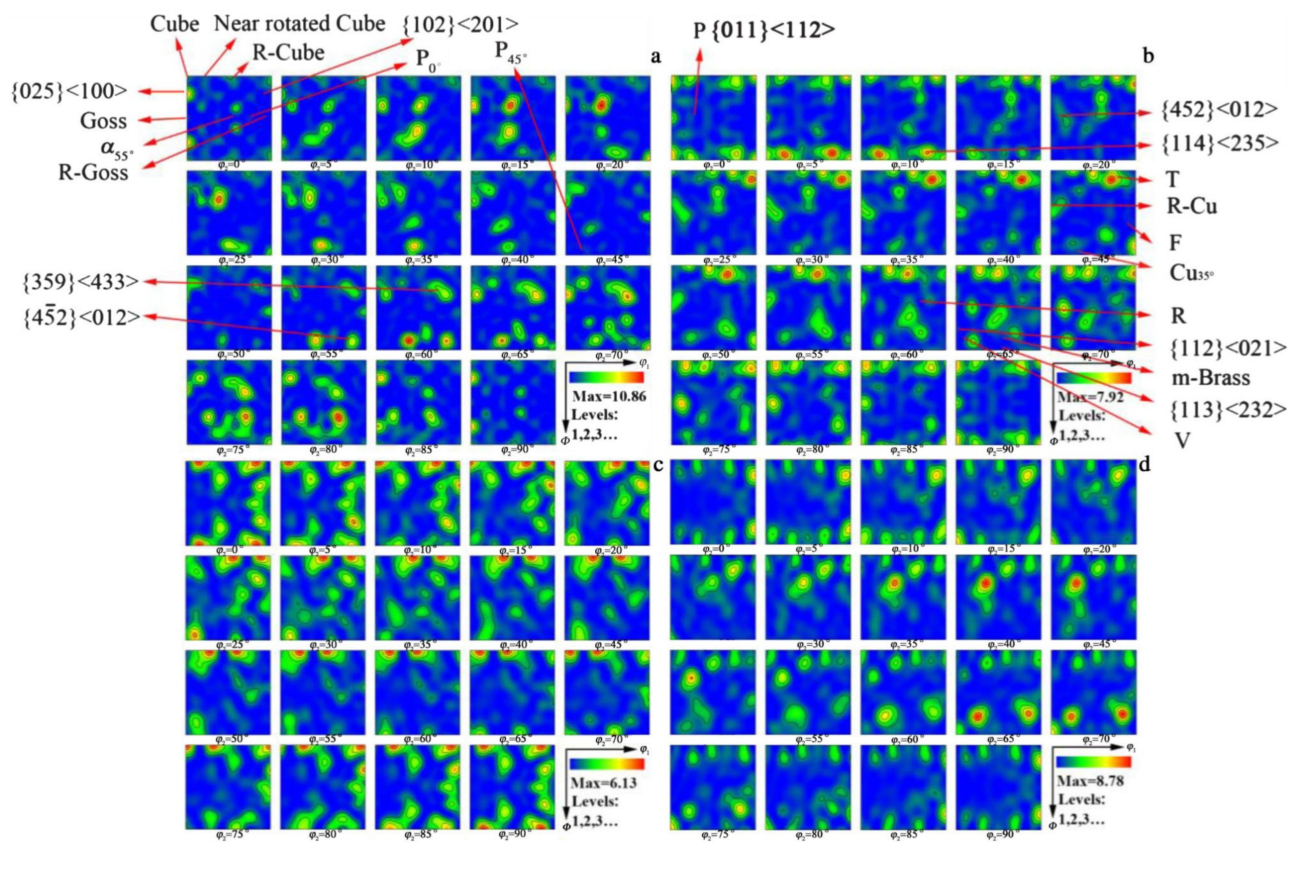

Fig.6 ODFs of 2A12 aluminum alloy after repeated deformation annealing: (a) 01#, (b) 11#, (c) 12#, and (d) 13#

Table 4 Texture type and intensity of 2A12 aluminum alloy after repeated deformation annealing

Texture type	Texture intensity			
	01#	11#	12#	13#
Cube	-	6.37	-	-
Near rotated Cube	-	7.92	6.13	6.16
Goss	-	5.89	-	-
m-Brass	4.78	3.35	-	-
$\alpha_{55°}$	9.87	-	-	-
T	-	7.3	6.13	-
F	4.18	-	-	-
R-Cu	4.83	-	-	-
V	-	-	-	8.36
{025}<100>	8.85	-	-	-
{359}<433>	8.69	-	-	-
{4$\bar{5}$2}<012>	8.73	-	-	-
{102}<201>	-	-	5.70	6.16
$P_{0°}$	-	-	3.14	-
$P_{45°}$			4.10	-
$Cu_{35°}$	10.86	-	-	-

Increasing the deformation amount can increase the deformed texture intensity after cold rolling, and also facilitate the formation of the annealed texture in the subsequent annealing process[21]. It is clear from the texture analysis results that the annealing process has a significant effect on the texture types of the repeatedly deformed annealed specimens. According to in Ref. [22], the Al-Cu-Mg alloy will exhibit the texture evolution path of the Brass, Goss, R-Goss, Cube during annealing. The intermediate textures created by the decomposition of brass are R-Cu and m-Brass. The texture evolution paths of samples 01# through 13# during repeated deformation and annealing are summed up as follows: when combined with the analysis findings of the ODF diagram: R-Cu and m-Brass→Goss→R-Goss→Cube, T and $P_{0°}$ →near rotated Cube and {102}<201>.

2.3 Effect of single-step deformation annealing on microstructure and texture of 2A12 alloy

2.3.1 Microstructure characteristics

The microstructure of 2A12 aluminum alloy samples after single-step deformation annealing is shown in Fig. 7. Grain boundary maps (Fig. 7b and 7e) and misorientation angle frequency histograms (Fig. 7c and 7f) show that 21# and 22# have primarily low angle grain boundaries. In 21# and 22# samples, the proportion of LAGBs (2°–15°) in total increases while the proportion of subgrain boundaries decreases compared to the proportion of HAGBs, LAGBs, and subgrain boundaries in sample 01#.

In general, compared to the low-temperature long-time annealing process, the high-temperature short-time annealing process produces a larger average grain size and more ideal equiaxial grains. Because when the deformation is the same, the high temperature annealing process can quickly release the deformation stored energy of the metal, resulting in higher recrystallization nucleation rates and faster grain growth rates. As a result, compared to 21#, 22# has a greater extent of recrystallization, larger grain size, and a higher proportion of HAGBs. The degree of recrystallization of the two single-step

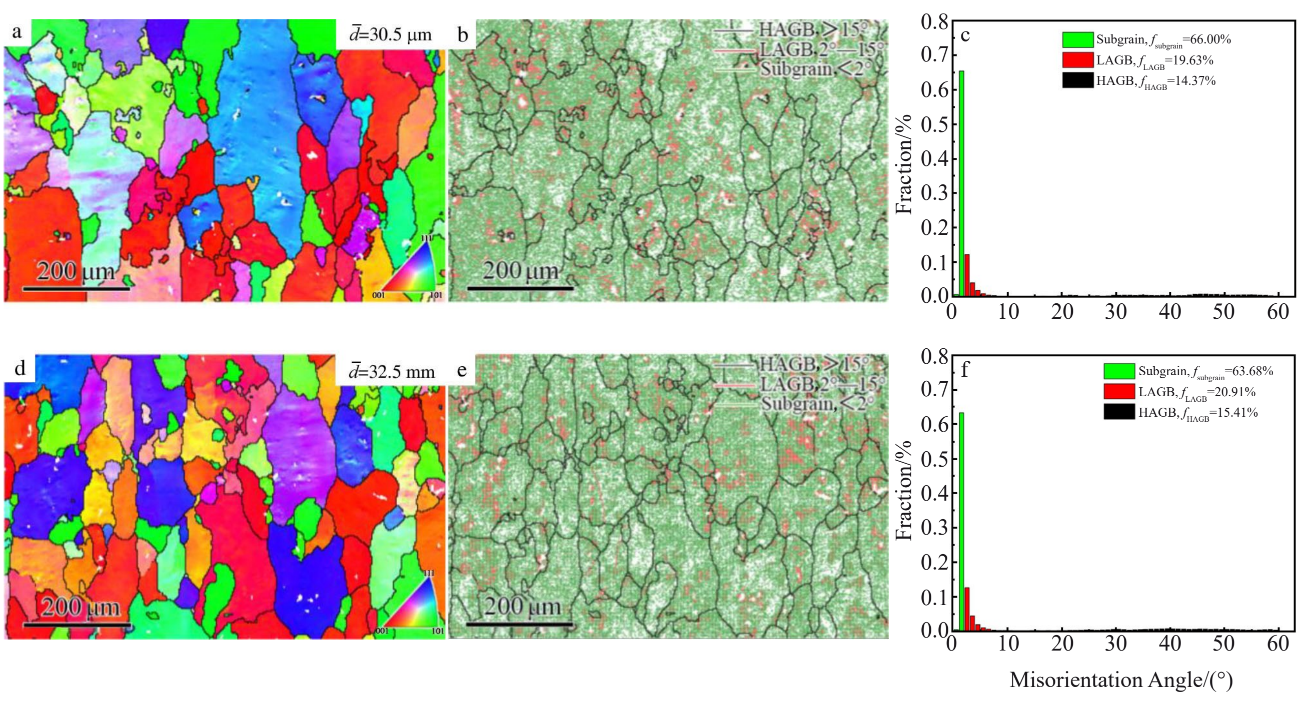

Fig.7 IPF maps, grain boundary maps, and misorientation angle frequency histograms of 2A12 aluminum alloy samples after single-step deformation annealing: (a–c) 21# and (d–f) 22#

deformation annealing samples is low, the proportion of HAGBs changes little, and the dislocation density and grain boundary ratio are close due to the small deformation of 5% and the constrained deformation energy storage.

2.3.2 Texture

Fig. 8 shows the ODFs of the samples after single-step deformation annealing. As shown in Fig. 8a and Table 5, 21# has a maximum intensity of 10.07, forming R-Cube, Goss, R{235} <833> , m-Brass, $Cu_{35°}$, R-Cu{112} <1$\bar{1}$1> , $\alpha_{55°}$, {025} <100> , {452} <012> , {4$\bar{5}$2} <012> and {112} <021> textures. 22# possesses a maximum intensity of 6.32, exhibiting the texture components consisting of R-Cube, R-Cu, F, and $P_{0°}$ components, as shown in Fig. 8b. Small deformation single-step annealing samples produce R-Cube texture as opposed to the Cube and near rotated Cube textures of previously repeated deformation annealing samples. This demonstrates that the texture evolution route will switch to R-Cu and m-Brass→Goss→R-Cube when the deformation is minimal.

2.4 Effect of large deformation annealing on microstructure and texture of 2A12 alloy

2.4.1 Microstructure characteristic

The IPF map for sample 31# is shown in Fig.9a. Despite the identical annealing process, 31# has a larger deformation extent, smaller grain size, a higher number of HAGBs broken during deformation, and forms more equiaxed crystals after annealing than 11#.

The grain boundary map (Fig. 9b) and misorientation angle frequency histogram (Fig. 9c) show that the proportion of LAGBs in total increases after large deformation annealing, the proportion of subgrain boundaries in total decreases, with little change in HAGBs, and the extent of recrystallization is higher than that of the 11# sample with 5% cold rolling deformation. The difference between the 11# and 31# samples demonstrates that the significant number of broken grains caused by large deformation will serve as nucleation sites for recrystallization and improve the extent of recrystallization after annealing.

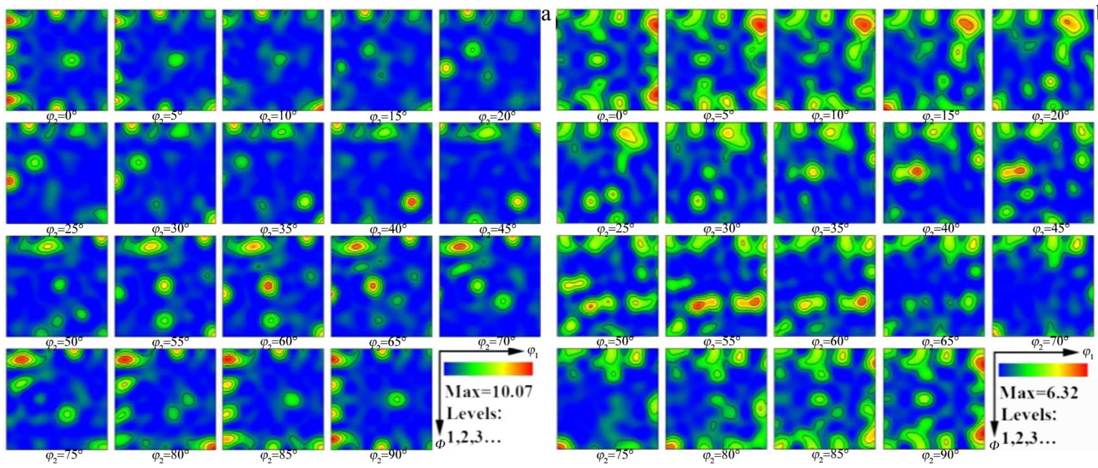

Fig.8 ODFs of 2A12 aluminum alloy after single-step deformation annealing: (a) 21# and (b) 22#

2.4.2 Texture

As shown in Fig. 10 and Table 6, sample 31# has a maximum intensity of 6.41, forming near rotated Cube, R-Goss, R-Cu, m-Brass, {102}<201> and T textures. The R-Cu and m-Brass textures in the original sample change to near rotated Cube and {102} <201> along the evolution path of repeated deformation and annealing. Some of them are reduced to Brass texture during large deformation cold rolling. The m-Brass intensity in the sample 13# with large deformation increases compared to the sample 11# with the same annealing system, and the R-Cu texture reappears. During subsequent annealing, the Goss texture is partly created by re-decomposing the Brass texture. As a result of repetitive deformation annealing and large deformation annealing, the texture evolution paths in the alloy are as follows: Brass→R-Cu and m-Bras→Goss→R-Goss→Cube, T

Table 5 Texture type and intensity of 2A12 aluminum alloy sample after single-step deformation annealing

Texture type	Texture intensity	
	21#	22#
Cube	10.07	6.32
R-Cube	7.48	3.77
Goss	7.63	-
R	8.47	-
m-Brass	4.41	
$Cu_{35°}$	3.85	-
R-Cu	4.76	5.62
α	3.72	-
F	-	5.56
P		3.48
{025}<100>	10.07	-
{4$\bar{5}$2}<012>	9.27	-
{452}<012>	9.38	-
{112}<021>	6.49	-

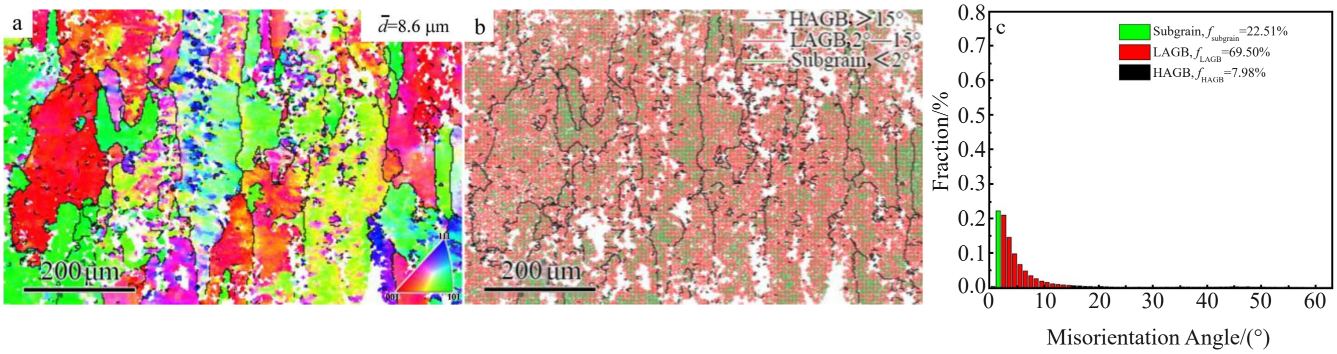

Fig.9 IPF map (a), grain boundary map (b), and misorientation angle frequency histogram (c) of 2A12 aluminum alloy sample 3# after large deformation annealing

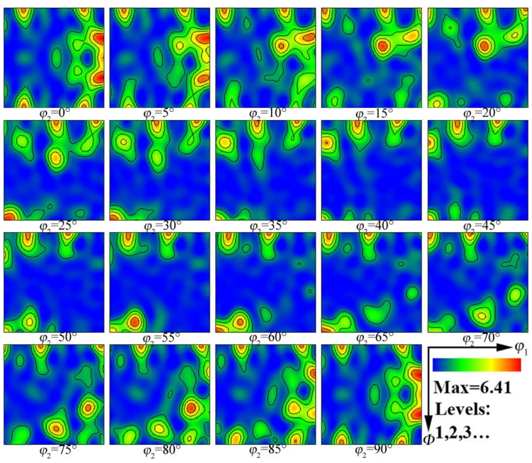

Fig.10 ODFs of 2A12 aluminum alloy sample 31# after large deformation annealing

Table 6 Texture type and intensity of 2A12 aluminum alloy sample 31# after large deformation annealing

Textures type	Texture intensity	Texture type	Texture intensity
Near rotated Cube	5.19	R-Cu	4.81
R-Goss	5.96	T	5.19
m-Brass	5.26	{102}<201>	6.41

and $P_{0°}$→near rotated Cube and {102}<201>.

2.5 Hardness and tensile properties

The influence diagram of various deformation annealing methods on the mechanical properties of 2A12 aluminum alloy is shown in Fig.11. Comparing mechanical properties of 11#, 12#, 13#, and 31# samples, it is clear that the alloy's mechanical properties get better as deformation increases.

The deformation of 13# and 31# is greater than that of 11#, the grain size decreases, the amount of the second phase increases, and the mechanical properties increase, as can be seen from the XRD pattern (Fig. 2) and the IPF diagram (Fig.3). The degree of recrystallization is low, the grain size is comparable, and the cold rolling deformation of the single-step deformation annealing samples of 21# and 22# is small. It

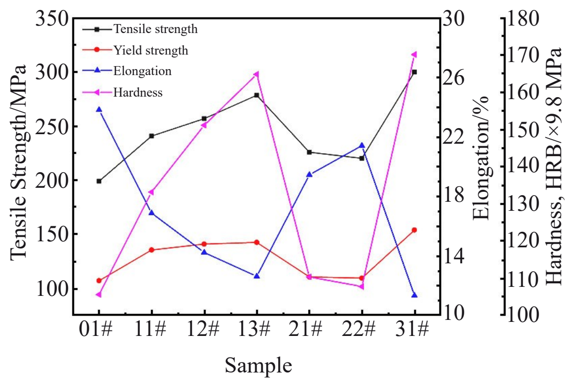

Fig.11 Microhardness and tensile properties of 2A12 aluminum alloy samples after deformation annealing

can be seen that the mechanical properties of the high-temperature annealed samples are inferior to those of the low-temperature annealed samples when compared with the results of the phase analysis of the cultural artifacts. The primary explanation is that the S phase is partially dissolved at high temperatures.

2.6 Electrochemical test

Fig. 12 and Table 7 exhibit the polarization curves of 2A12 aluminum alloy after deformation annealing and their fitting

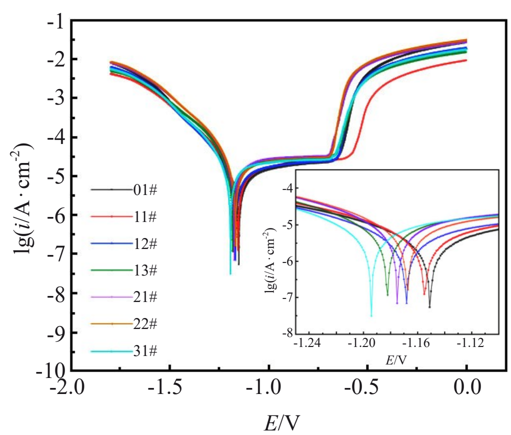

Fig.12 Polarization curves of 2A12 aluminum alloy samples after deformation and annealing

Table 7 Fitting parameters obtained from Tafel polarization curves

Sample	E_{corr}/VSCE	I_{corr}/×10^{-5} A·cm^{-2}	R_p/Ω·cm^2
01#	−1.151	0.7718	5240.5
11#	−1.155	0.986	42817
12#	−1.168	0.8981	4537.4
13#	−1.182	1.689	2569.7
21#	−1.175	1.958	2260.5
22#	−1.167	1.676	2582.0
31#	−1.194	1.477	2962.3

findings. The more positive the corrosion potential, the lower the corrosion current, and the higher the polarization resistance of the material, the better the corrosion resistance. According to the above standards, sample 01# has the best corrosion resistance, while sample 31# has the lowest corrosion resistance. The corrosion resistance of the samples is ranked in descending order: 01#, 11#, 22#, 12# and 21#.

2.7 Exfoliation corrosion test

The curve of mass loss and test time was simulated using Eq.(1), and the results are shown in Table 8 and Fig.13.

$$M = At^B \quad (1)$$

where M is mass loss (g/m^2), t is test time (h), and A and B are constants.

The correlation coefficients R^2 of the samples are all close to 1, indicating that the fitting results are reasonable. The mass losses of the samples are ranked in ascending order: 01#, 11#, 22#, 12#, 21#, 13#, and 31#. This result is identical to the electrochemical test results.

Table 8 Corrosion kinetic empirical function of 2A12 aluminum alloy samples

Sample	Empirical function	Correlation coefficient, R^2
01#	M=1.74$t^{0.6}$	0.998
11#	M=1.8$t^{0.66}$	0.991
12#	M=5.12$t^{0.52}$	0.999
13#	M=7.2$t^{0.51}$	0.994
21#	W=5.78$t^{0.54}$	0.997
22#	M=4.12$t^{0.51}$	0.992
31#	M=7.87$t^{0.5}$	0.997

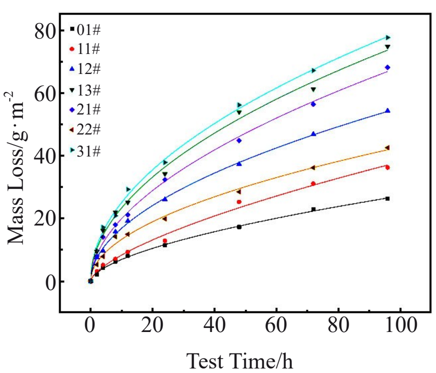

Fig.13 Experimental and fitting curves of mass loss and test time of 2A12 aluminum alloy samples in EXCO solution

Table 9 shows the visual ratings of all seven corroded samples immersed in EXCO solution for various time. Sample 12#, 13#, 21#, and 31# exhibit high corrosion susceptibility during the initial stage of exfoliation corrosion (0–12 h). Their ratings all developed to EA successively, whereas for 01#, 11# and 22# samples, which have better corrosion resistance, their ratings stay mostly between PA and PC. At this point, the visual evaluation is essentially in agreement with the electrochemical test results. The ratings of 12#, 13#, 21#, and 31# samples remain at EA level in the late stage of exfoliation corrosion (12 – 96 h). Compared with sample 01#, 11#, and 22#, sample 12#, 13#, 21#, and 31# exhibit a lower degree of exfoliation corrosion, which may be because their surface metal layers peel off too quickly. According to the exfoliation corrosion mechanism, the grains of 2XXX series aluminum alloy will be elongated along the rolling direction after the cold rolling deformation. When grain boundaries parallel to the material surface are corroded, and intergranular microcracks are formed, and the loose corrosion products cause a "wedge effect", i.e., strata forms wedges of corrosion products that force layers of metal upward, giving rise to a layered appearance[23]. The upper layer of metal is lifted and eventually separated from the substrate as the corrosion products gradually penetrate deeper into the sample. Significant delamination may not be observed if the surface metal peels off too quickly and the size of the separate metal layer is too small.

After the exfoliation corrosion test, a substantial amount of metal powder is found at the bottom of the containers of sample 12#, 13#, 21#, and 31#. This phenomenon indicates a significant degree of surface metal peeling in the four samples of 12#, 13#, 21#, and 31#, which is why no evident delamination is found on the surface of these four samples.

Combining the preliminary analysis results, it is clear that 13# and 31# samples contain more second phases, which cause galvanic corrosion between the second phase and the matrix to be severer and make the pitting corrosion to

Table 9 Visual ratings of 2A12 aluminum alloy samples immersed in EXCO solution for various time after deformation annealing

Corrosion time/h	Visual rating						
	01#	11#	12#	13#	21#	22#	31#
2	PA	PA	PC	PC	PC	PA	PC
4	PA	PB	PC	EA	EA	PB	EA
8	PB	PB	EA	EA	EA	EA	EA
12	PC	PC	EA	EA	EA	EA	EA
24	PC	PC	EA	EA	EA	EB	EA
48	EA	EB	EA	EA	EA	EC	EA
72	EA	EB	EA	EA	EA	ED	EA
96	EB	EC	EA	EA	EA	ED	EA

progress more rapidly. It is easy to cause exfoliation corrosion because the alloy retains the broken and elongated grains produced by significant deformation. Compared to 13# and 31# samples, the second phase is reduced, the grain elongation is lower, and the corrosion resistance is increased. Samples 01#, 11#, and 22# have greater corrosion resistance due to lower second phase content and lower grain deformation.

3 Conclusions

1) After deformation annealing, the grains of 2A12 aluminum alloy are elongated along the rolling direction, and the grain size decreases. The proportion of subgrain boundaries decreases, the proportion of LAGBs (2° – 15°) increases, and the proportion of HAGBs increases first and then drops with an increase in repeated deformation annealing cycles. Recovery multi-lateralization gives way to recrystallization during the heating process, and the degree of recrystallization rises. Because of the low deformation and less deformation stored energy, the proportion of distinct grain boundaries and microstructures in 21# and 22# samples is similar. Compared to sample 11# with the same annealing process, the sample 31# has a smaller proportion of subgrain boundaries, LAGBs and HAGBs increase and the degree of recrystallization increases.

2) The route taken by the texture of 2A12 aluminum alloy during large deformation annealing and repeated deformation annealing is as follows: Brass→R-Cu and m-Brass→Goss→R-Goss→Cube, T and $P_{0°}$ →near rotated Cube and {102}<201>. When the deformation is small, the path will change to: R-Cu and m-Brass→Goss→R-Cube.

3) The strength and hardness of 2A12 aluminum alloys increase with increasing deformation, while the toughness and plasticity decrease. Sample 01# has the best exfoliation corrosion property and electrochemical properties, while sample 31# has the worst. Samples 12#, 13#, 21#, and 31# will have a lower degree of visual evaluation at the late stage of exfoliation corrosion than samples 01#, 11#, and 22#.

References

1 Wang C, Su Y, Ouyang Q *et al. Vacuum*[J], 2021,188: 110 150

2 Deng Y, Jia H, Li J. *Materials Today Communications*[J], 2022, 30: 103 118

3 Jiang J, Zhang Y, Wang Y *et al. Materials & Design*[J], 2020, 193: 108 859

4 Dadbakhsh, Karimi Taheri A, Smith C W. *Materials Science and Engineering A* [J], 2010, 527(18–19): 4758

5 Zhong X X. S*tudy on Microstructure and Properties of Fine Grain 2A12 Aluminum Alloy Prepared by High Pressure Torsion*[D]. Hebei: Yanshan Unibersity, 2021 (in Chinese)

6 Ma G, Ling H, Liu Z *et al. Rare Metal Materials and Engineering*[J], 2022, 51(9): 3166

7 Li N, Li G, Nie B *et al. Aluminum Alloy Materials and Its Heat Treatment Technology*[M]. Beijing: Metallurgical Industry Press, 2012: 221 (in Chinese)

8 Guo Yunyue. *Optimization of Solution and Aging Heat Treatment Parameters of Cold-Rolled 2024 Aluminum Alloy Sheets*[D]. Jinan: Shandong University, 2019 (in Chinese)

9 Wang T, Huang Y, Ma Y *et al. Journal of Materials Research and Technology*[J], 2021, 15: 3337

10 Xu Gong. *Investigation on Microstructure and Mechanical Property of Al-Cu Alloy During Process of Deformation and Recrystallization*[D]. Chongqing: Chongqing University, 2013 (in Chinese)

11 Hu Zeyi. *Study on the Mechanisms of Forming Strengthening and Toughening in the A1-Cu-Mg Alloy for Special Packaging*[D]. Zhuzhou: Hunan University of Technology, 2021 (in Chinese)

12 Tang Hua. *Studies on Technology and Properities of Hard Anodizing of 2A12 Aluminum*[D]. Nanchang: Nanchang Hangkong University, 2011 (in Chinese)

13 Xiao K, Nie W, Jian H *et al. Journal of Hunan University of Technology*[J], 2022, 36(4): 39 (in Chinese)

14 Afseth A, Nordlien J H, Scamans G M *et al. Corrosion Science*[J], 2002, 44(11): 2491

15 Afseth A, Nordlien J H, Scamans G M *et al. Corrosion Science*[J], 2001, 43(11): 2093

16 Xue D, Wei W, Shi W *et al. Journal of Materials Research and Technology*[J], 2021,15: 6329

17 Wang B, Chen X H, Pan F H *et al. Transactions of Nonferrous Metals Society of China*[J], 2015, 25: 2481

18 Tayyaba Q, Butt A Q, Shahzad M *et al. Metallurgical and Materials Engineering*[J], 2022, 28: 319

19 Ling M. *Study on the Effect of Solution and Aging Treatment Process on Microstructure and Mechanical Properties of Cold Rolled 2A12 A1 Alloy Sheet*[D]. Jinan: Shandong University, 2019 (in Chinese)

20 Shen F, Li W, Sun Z *et al. Journal of Alloys and Compounds*[J], 2021, 871: 159 613

21 Chen Y, Xiong C, Liu W *et al. Applied Sciences*[J], 2021, 11(12): 5550

22 Huang T, Liu F, Liu Z *et al. Journal of Materials Engineering and Performance*[J], 2022, 31: 1419

23 Mu C, Wen Q, Feng W *et al. Aluminum Fabrication*[J], 2020, 5: 9 (in Chinese)

形变热处理对2A12铝合金微观组织、织构及性能的影响

蹇海根[1,4]，肖可谋[1,3]，牌君君[2]，陈　淼[1]，张　唯[3]

(1. 湖南工业大学 材料与先进制造学院，湖南 株洲 412007)

(2. 山东省先进铝基材料与技术重点实验室，山东 滨州 262207)

(3. 广东峰华卓立科技股份有限公司，广东 佛山 528200)

(4. 欧科亿数控精密刀具股份有限公司，湖南 株洲 412500)

摘　要：利用扫描电镜显微观察（含能谱分析）和电子背散射衍射技术（Electron Backscatter Diffraction， EBSD）等分析方法研究了不同形变热处理制度对2A12铝合金板材的微观组织、织构及性能的影响。结果表明：2A12铝合金经形变热处理后，晶粒沿轧制方向拉长，晶粒尺寸减小。随着形变热处理反复次数的增加，亚晶界比例降低，2°–15°的小角度晶界比例提高，大角度晶界比例先增后减，此时的退火过程由回复多边化主导转变为再结晶主导，再结晶程度提高。单步形变热处理样品因形变量较小，大小晶界和亚晶界比例较为接近。与退火制度相同的小变形样品相比，大形变热处理样品亚晶减少，大角度和小角度晶界增加，再结晶程度提高。形变量较大时，将存在Brass→R-Cu和m-Brass→Goss→R-Goss→Cube、T和$P_{0°}$→Near rotated Cube和｛102｝<201>的织构演变路径。单步小变形退火时，路径将改变为：R-Cu和m-Brass→Goss→R-Cube。随着变形量的增加，2A12铝合金的强度和硬度增加，韧性和塑性降低。

关键词：2A12铝合金；形变退火；力学性能；腐蚀性能；织构

作者简介：蹇海根，男，1980年生，博士，教授，湖南工业大学材料与先进制造学院，湖南 株洲 412007，电话：0731-22183451，E-mail：jianhaigen2001@163.com